The Central kpc of Starbursts and AGN
ASP Conference Series, Vol. xxx, 2001
J. H. Knapen, J. E. Beckman, I. Shlosman, and T. J. Mahoney

Dynamics of the Central kpc in Barred Galaxies: Theory and Modeling

Isaac Shlosman[1,2]

Joint Institute for Laboratory Astrophysics, University of Colorado, Campus Box 440, Boulder, CO 80309-0440, USA

Abstract. The central kpc of barred galaxies exhibits a wealth of morphological information on different components with clear dynamical consequences. These include nuclear rings, spirals, bars, and more. We argue that this morphology is driven by large-scale stellar bars and analyze its consequences for gas dynamics and the distribution of star-forming regions. Specifically, we focus on gas flows in nested bar systems and study their origin, as well as the gravitational decoupling of gaseous nuclear bars with and without gas self-gravity. We find that the gas response in nested bars differs profoundly from that in single bars, and that no offset dust lanes form in the nuclear bars.

1. Introduction

For years, disk galaxies have been studied with unresolved centers, called nuclei, of up to a few kpc in size. Recent progress in ground-based instruments and the availability of the *Hubble Space Telescope* (*HST*) has allowed for the first time a meaningful analysis of central morphology and kinematics, both stellar and gaseous. Although our knowledge of the inner regions of disk galaxies is clearly incomplete, certain patterns in their dynamical evolution and their relationship to larger and smaller spatial scales have emerged.

At least dynamically, the inner parts of disk galaxies can be defined by the position of the inner Lindblad resonance(s) (hereafter ILRs), typically at about 1 kpc from the center. This resonance between the bar pattern speed and the precession rate of periodic orbits plays an important role in filtering density waves, either stellar or gaseous, propagating between the bar corotation radius and the center (e.g., Binney & Tremaine 1987). It is usually delineated by elevated star formation rates and the concentration of molecular gas in one or more nuclear rings. These rings exhibit a rich morphology and can serve as cold gas reservoirs for fueling the central activity, stellar and non-stellar.

It is a well-known property of rotationally supported gravitational systems that any departure from axial symmetry facilitates angular-momentum transfer

[1] JILA Visiting Fellow.

[2] Permanent address: Department of Physics and Astronomy, University of Kentucky, Lexington, KY 40506-0055.

due to gravitational torques across large radial distances. The action of torques can be described in terms of non-local gravitational viscosity and can be very efficient, when the departures from axisymmetry are substantial, driving the dynamical and secular evolution of these systems. Numerous effects of such evolution have been detected in barred galaxies, ranging from making them more centrally concentrated by driving the gas inwards, to reducing radial abundance gradients. In the absence of non-axisymmetric perturbations, the dynamical evolution is expected to slow down dramatically.

The above effects are due to large-scale stellar bars and have been extensively studied during the last two decades. Gravitational torques and other effects of such bars are most prominent on scales of several kpc, where the ratio of non-axisymmetric-to-radial force peaks. At smaller galactocentric distances the influence of these bars decreases dramatically, and within the central kpc, inside the ILR(s), the bar potential becomes more axisymmetric. The question then is, What is the prime factor driving evolution in these regions, where the effects of large-scale bars are weak?

Here we review the basic morphologies of the central kpc in *barred* galaxies and analyze the possible dynamical role of nuclear rings, nuclear spirals and nuclear bars. This is done using high-resolution *HST* and ground-based observations of the last few years. In most cases these morphological features are secondary, in the sense that they have been caused, directly or indirectly, by large-scale bars.

2. Nuclear Rings and Large-Scale Bars: The Global Connection

The gas response to the gravitational torquing of the large-scale bar depends mainly on the galactic mass distribution and the pattern speed of the bar, which determine the positions of the major resonances in the disk. For a wide range of bar properties, the gas response is characterized by offset dust lanes delineating large-scale shocks, which are stationary in the bar frame of reference and govern the gas flow in the bar (Prendergast 1962). Athanassoula (1992) has presented a quantitative analysis of the flow pattern between the ILRs and the corotation and has shown that the existence of one or two ILRs is necessary to produce shocks which are offset from the bar major axis. In the absence of even one ILR, the shocks are centered on the axis. The subsequent search in the RC3 catalogue (de Vaucouleurs et al. 1991) has revealed only a couple of barred galaxies which exhibit centered shocks (E. Athanassoula, private communication). The shape of the offset dust lanes depends on the bar strength; stronger bars are accompanied by straight dust lanes without star formation, while weaker bars show curved lanes with some star formation. Gas enters the shocks (roughly) perpendicularly, and afterwards follows their outline, leading to a strongly radial inflow towards the ILRs.

Across the ILR(s), shocks curve and become more circular, which results in a shock-focused, azimuthal flow. Each ILR is characterized by a pair of shocks, e.g., trailing at the outer ILR, leading at the inner ILR, and again trailing at the nuclear Lindblad resonance (NLR), if one exists (Fig. 1). Reduction in the radial inflow velocity leads naturally to gas accumulation at the above radii, which form so-called nuclear rings.

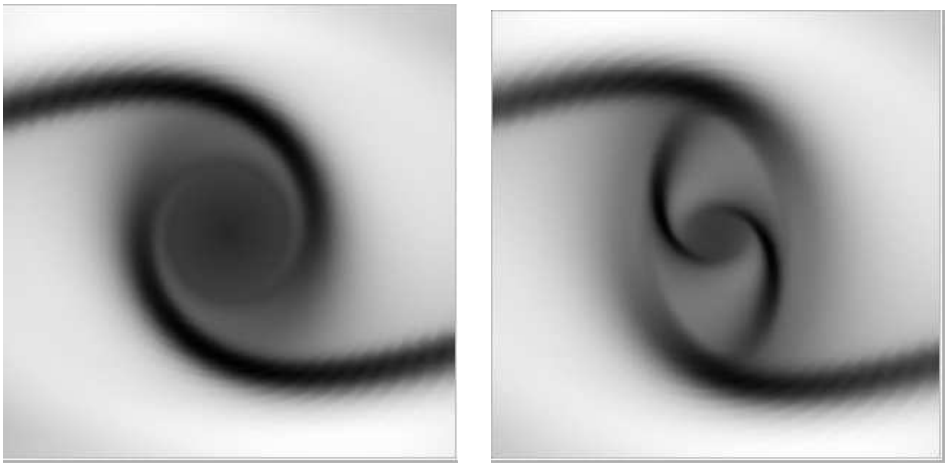

Figure 1. *Grayscale* gas response to stellar bar torque. The bar is horizontal and rotation is clockwise in its frame. Only the central resonance region of 2 kpc is shown. *Left:* A single ILR is present causing a pair of trailing spirals to form. The innermost gas settles on nearly circular x_2 orbits in an undisturbed nuclear disk. *Right:* A pair of ILRs is present, causing two pairs of spirals to form, a leading and a trailing one. (*From Shlosman 1999.*)

The origin of the offset shocks in the presence of ILRs can be easily understood from the orbit analysis. With no ILRs, stationary periodic orbits, which exist in the bar frame, are all aligned with the bar major axis (hereafter x_1 orbits; Contopoulos & Papayannopoulos 1980). Although the internal dissipation in the gas leads to energy loss, one can still predict the major features of gas response knowing the major families of periodic orbits in the bar. At each ILR, the orbits change their alignment by $\pi/2$. Hence between the ILRs (or between the center and the ILR, if only one exists) the orbits are aligned with the minor axis of the bar (hereafter x_2 orbits). Stars can change their orbits abruptly, while gas can do this only gradually by forming a pair of shocks.

The most important observed characteristics of nuclear rings are: a) their mass, typically in the range of 10^8–a few $\times 10^9$ $M_\odot$ in molecular gas; b) their single or double appearance; c) their location close to the turnover velocity; d) their oval or circular shapes leading the bar in the first quadrant; and e) accompanying star formation in the inner part of the ring. Theoretically, nuclear rings are indeed subject to fragmentation and star formation (Elmegreen 1994). This has been confirmed by numerical modeling, which has shown also that the ring shapes, orientation, colors, and star formation distribution depend on the rate of gas inflow from larger radii (Knapen et al. 1995). Moderate or high rates of inflow result in a characteristic oval shape of the ring, with its major axis leading the bar by about 50°–80°, and with two or four prominent sites of star formation, depending on whether one or two ILRs exist (two star-forming regions on the bar minor axis and two on the bar major axis, respectively, see Fig. 2). On the other hand, low inflow rates result in much rounder and redder rings, with a smoother distribution of star formation. In fact, no ring is found

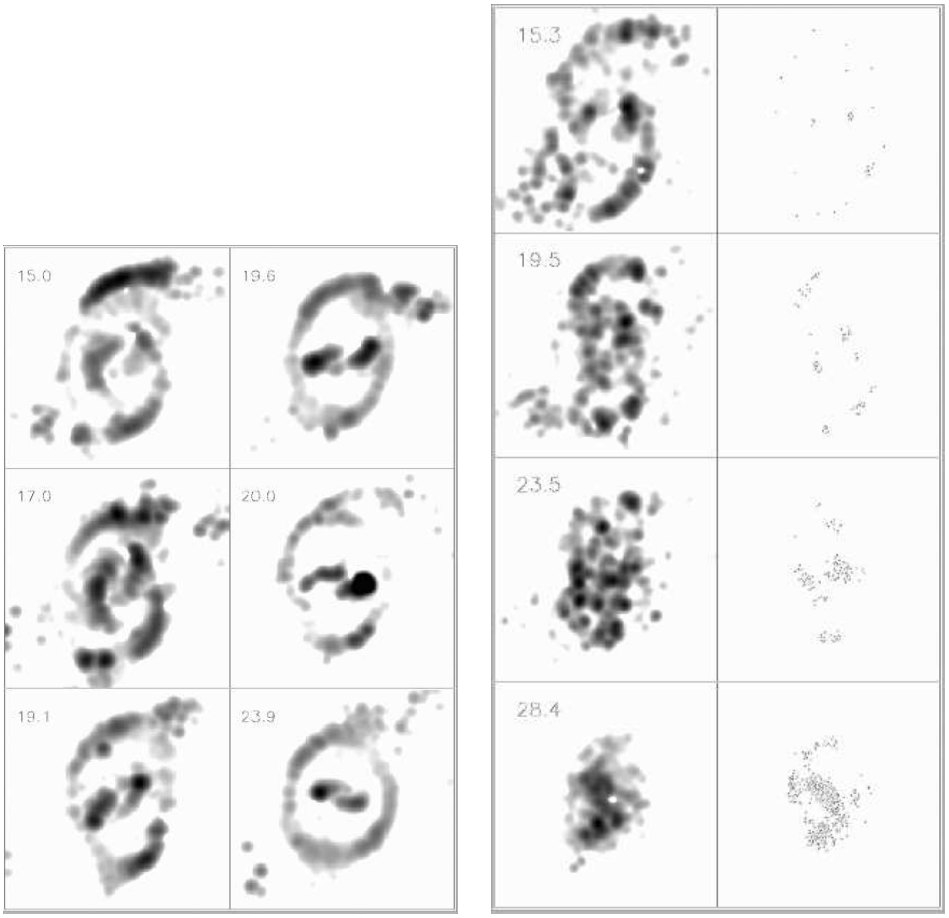

Figure 2. Self-gravitating gas in self-consistent simulations of a 3D gas + stars disk (shown face on). Logarithmic *grayscale* map of shock dissipation without (*1st and 2nd columns*) and with (*3rd column*) star formation in the central kpc of a barred galaxy with two ILRs. Time in bar rotations is given in the *upper left corners*. The stellar bar is horizontal and rotation is anti-clockwise. The *right* (*4th*) *column* is a star formation map corresponding to the *third column*. Inclusion of star formation causes both nuclear rings to merge and shows the subsequent gas inflow (last frame at 28.4) across the inner ILR. (*From Knapen et al. 1995.*)

to be sitting close to the outer ILR; rather, it is positioned half way between the ILRs. If more than one ring is formed, rings can interact both hydrodynamically and gravitationally (Heller, Shlosman, & Englmaier 2001; see also §4.1).

Star formation increases the rate of viscous dissipation in the ring by supporting turbulent motions in the gas. This appears to be one of the factors capable of shrinking the ring radially and driving an inflow across the inner ILR that is otherwise prevented due to the change in the direction of the torque interior to the ring.

Massive nuclear rings have been found to affect the stellar and gas dynamics, in and out of the disk plane (Heller & Shlosman 1996). This happens mainly by: i) strengthening (or creating) double ILRs; ii) making the x_1 orbits interior to the ring less eccentric; iii) increasing the phase space occupied by the x_2 orbits; and iv) skewing the x_1 orbits outside an ovally shaped ring, misaligned with the bar major axis. This leads to orbit intersection and depopulates them of the gas, which falls towards the ring.

Increasingly massive nuclear rings push the outer ILR outwards, weakening the stellar bar between the ring and corotation. When the outer ILR radius becomes comparable to the bar minor axis, most of the orbits supporting the bar potential disappear and the bar is expected to dissolve, leaving a weakened bar remnant inside the inner ILR. Such bars, extending to the ILRs are found in late-type disk galaxies (Elmegreen & Elmegreen 1985), with no active star-forming rings encircling them. Bar dissolution outside the nuclear ring will cut off gas inflow which fuels the star formation, although aged stellar rings will survive dynamically (Shlosman 1999). Such red "fossil" rings have been found recently in a number of disk galaxies (Erwin, Vega Beltrán, & Beckman, this volume, p. 171).

To summarize, nuclear rings are clear signatures of large-scale stellar bars and of the availability and recent radial transport of large quantitites of molecular gas by means of gravitational torques.

3. Nuclear Bars and Nuclear Spirals: Gas Dynamics

3.1. Gas Density Waves Within the Central kpc

Two new morphological features can play a dominant role in the central regions of disk galaxies. Recent high-resolution observations of galactic centers revealed a number of paired, grand-design spirals (Laine et al. 1999; Martini & Pogge 1999; Regan & Mulchaey 1999). Because most barred galaxies seem to possess at least one ILR, and stellar density waves are damped and cannot propagate across it, what drives the observed nuclear spiral structure? One can be motivated by the fact that these spirals are notable in near-infrared colors (of dust) and do not seem to be associated with a high level of star formation. In addition, the inner spiral structure appears to be a continuation of the outer spirals and shows low arm-interarm contrast. The above constraints allow for an alternative explanation of grand-design two-arm spiral structure in the centers of disk galaxies by means of gas density waves (Englmaier & Shlosman 2000). These can freely propagate across the resonances. Probably the most interesting result is that the shape of the nuclear spiral, i.e., its pitch angle, depends on the shape of the gravitational potential and on the sound speed in the gas, hence providing an insight into the mass distribution at several hundred pc from the center and into possible conditions in the ISM. The shape of the nuclear spiral requires a gently rising rotation curve and hence a low central-mass concentration.

We specifically target the case where the large-scale perturbation is caused by the stellar bar and therefore assume dominant barlike modes with $m = 2$. This approach can be generalized for any symmetry of the perturbation. For a certain range of central concentrations and sound speeds, $c_{\rm s}$, the gas response generates a spiral pattern between the corotation and the center, winding into

Figure 3. *Grayscale* image of a steady-state gas response to the bar perturbation in a model with mild central concentration (only the inner 2 kpc are shown). The stellar bar is horizontal and extends to 5 kpc and the ILR is at 2 kpc; the gas rotates clockwise. The sound speed is 10 km s^{-1}. (*From Englmaier & Shlosman 2000.*)

an unusual angle of $\sim 3\pi$ radian (Fig. 3). Part of the pattern corresponding to the winding of π radians, i.e., between corotation and the first crossing of the bar major axis, is a strong standing shock in the bar frame. We refer to the radius when the shock first crosses the bar major axis as a transition radius, $R_{\rm t}$. The spiral pattern is formed by the gas moving from x_1 to x_2 orbits, which was confirmed by means of non-linear orbit analysis (described in Heller & Shlosman 1996). The modeled gas response in Fig. 3, however, clearly shows continuation of the spiral pattern well past the region of expected winding.

To understand the reason for the observed gas response and the large winding angle, we compare the density response amplitudes along the spirals (Fig. 4, *left*). This amplitude decreases substantially after the first π, counting from the corotation inwards, i.e., inside the $R_{\rm t}$. Such a decline means that the shock strength drops sharply, and that the gas response at smaller radii is more of a linear wave and is consistent with the gas settling on the x_2 orbits. The initial π winding corresponds to this process. At smaller radii, additional driving must support the modeled spiral pattern, a process that requires a milder orbital change.

The spiral pattern in Fig. 3 is stationary in the bar frame. Viewed in the fluid rest frame at some R, the radial component of the wave vector points inwards because the gas rotates faster than the spiral pattern everywhere inside the corotation. It is convenient to explain the spiral in terms of a wave packet propagating radially inwards, which is sheared by the differential rotation in the disk. The only waves which can propagate inside the ILR are the short waves,

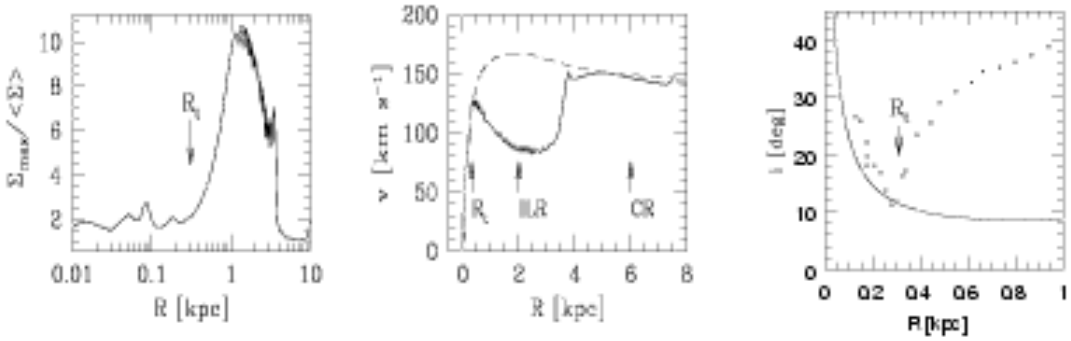

Figure 4. *Left:* Spiral-arm surface density normalized by the average density at radius R for the standard model. The *vertical arrow* shows the position of a transition radius $R_{\rm t}$, where the spiral pattern winds up the initial angle of π (measured from corotation). The spiral weakens substantially inside $R_{\rm t}$ and outside 4 kpc where it crosses the bar axis again. Shocks in the outer spiral ($> R_{\rm t}$) are unresolved, thus the surface density plotted here is only a lower limit. *Center:* The gas azimuthal velocity component (*solid line*) measured along the spiral in the inertial frame. Circular velocity for the axisymmetric part of the potential (*dashed line*) is shown for comparison. The gas is on nearly circular orbits inside $R_{\rm t}$ and outside 4 kpc, and transits from x_1 to x_2 orbits in between. *Right:* Spiral pitch angle vs. R. Theoretical (*solid line*) and modeled (*dots*) curves are shown. (*From Englmaier & Shlosman 2000.)*

and their group velocity is slower than the sound speed, due to the contribution of the epicyclic motion.

The low arm–interarm contrast observed in the model inside $R_{\rm t}$ (Fig. 4, *left*) confirms that the wave is not accompanied by a strong compression. This is in agreement with observed nuclear spirals, which do not exhibit extensive star formation and are mainly seen because of the dust obscuration, and justifies our ignoring self-gravitational effects in the gas. The pitch angle of the innermost spiral pattern decreases quickly with radius, i.e., the pattern becomes tightly wound. This is in sharp contrast with the pitch angle at $R > R_{\rm t}$, which corresponds to the x_1-to-x_2 orbital switch. Here the pitch angle quickly increases with radius, and the overall response becomes open. The wedge-shaped profile of the pitch angle in Fig. 4 (*right*) is therefore characteristic of switching from one type of response to another.

Both responses cannot coexist at the same radii. Moving inwards from the ILR, the spiral pattern associated with the outer shocks winds round the center and the pitch angle decreases. At some value $R_{\rm t}$, the low-amplitude density waves take over and slowly increase this angle. The gas can only sustain waves of a particular frequency at each R; these are solutions to the dispersion

relationship. Therefore, the solutions for the pitch angle can only switch from the inner to the outer one where they are comparable.

Importantly, there is a strong dependence of the spiral shape in the nuclear region on the central concentration. A factor of 2 increase in central concentration makes the spiral pattern so tightly wound that it is not recognizable any more beyond the initial winding of π. This results in the formation of a featureless nuclear disk within the inner 400–500 pc. For smaller central concentrations, the spiral becomes less tightly wound and finally collapses towards the bar's major axis. The modeled gas responds in a non-linear fashion, staying on x_1 orbits inside the weak ILR. We have observed this effect, which leads to the formation of shocks centered on the major bar axis. Its strength depends also on the sound speed in the gas. This effect has been studied independently by Englmaier & Gerhard (1997) and Patsis & Athanassoula (2000).

The measured pitch angle, i, of the modeled spiral is given by dots in Figure 4 (*right*). We observe a twofold behavior for i; from the ILR inwards it is decreasing until the shock pattern winds the angle of π ($R_{\rm t}$, indicated by an arrow), and then starts to unwind. Remarkably, there is a sharp break in the $i(R)$ slope at this point. The inner part of the $i(R)$ curve is in agreement with theory. As we have noted above, the outer part of the $i(R)$ curve describes the non-linear gas response to the bar forcing. Figure 4 (*right*) demonstrates that the large-scale shock penetrates inside the ILR and perturbs the nuclear gas disk. Hence, it is the large-scale shock which directly drives the nuclear spiral structure.

Figure 4 (*middle*) displays the azimuthal velocity component of the gas flow measured along the spiral arm. Inside the transition radius, $R_{\rm t}$, the azimuthal gas velocity is very close to the rotational velocity in the axisymmetric potential (dashed line). Somewhat farther out, the tangential velocity shows a sharp drop, due to the non-circular motions in the gas which is in the process of settling into x_2 orbits. This demonstrates the observational significance of the transition radius, $R_{\rm t}$; namely, it represents the outer radius of the nuclear disk where the gas is found in nearly circular x_2 orbits aligned with the minor axis of the bar. The deviation from the axisymmetric rotation curve is greatest around the ILR radius. Furthermore, the bar-driven shocks reach the bar major axis again at ~ 4 kpc. Beyond this radius, the gas follows nearly circular orbits.

An alternative way to explain nuclear spirals exists, at least in principle, and requires a strong central-mass concentration in the form, for example, of a supermassive black hole (SBH). One might expect that the SBH not only contributes its own mass but affects the nearby stellar density distribution as well—a kind of gravitational "polarization" effect which encompasses a factor of ten more mass than the SBH. This will lead to the formation of an additional (NLR) resonance and a pair of trailing spirals (Shlosman 1999) that can have an appearance of grand-design nuclear arms.

In the first case, the nuclear spirals are not expected to have a strong effect on the radial gas redistribution due to their low amplitude. This may not be true in the latter case, as the shocks will quickly move the gas across the NLR.

3.2. Nested Bars

A morphological feature that is expected to dramatically affect the gas dynamics inside the central kpc is a nuclear bar. Although these sub-kpc bars have been probably detected by de Vaucouleurs (1974), Sandage & Brucato (1979), and Kormendy (1982) as optical isophote twists in the central regions of barred galaxies, they have been interpreted as triaxial bulges. High resolution ground-based observations have revealed a number of galaxies with small bars residing within the large-scale stellar bars (e.g., Buta & Crocker 1993; Shaw et al. 1995; Friedli et al. 1996; Jungwiert, Combes, & Axon 1997; Mulchaey & Regan 1997; Elmegreen, Chromey, & Santos 1998; Jogee, Kenney, & Smith 1998; Erwin & Sparke 1999, Knapen, Shlosman, & Peletier 2000; Emsellem et al. 2001; Laine et al. 2001). The molecular gas content of these bars varies. In some cases, the cold gas can be dynamically important, as evident from the 2.6 mm CO emission and NIR lines of H_2 (e.g., Ishizuki et al. 1990; Devereux, Kenney & Young 1992; Kotilainen et al. 2000; Maiolino et al. 2000). Depending on the gas fraction contributing to the gravitational potential, one can distinguish stellar- or gas-dominated and mixed nuclear bars. The largest sample (112) of disk galaxies analyzed so far for this purpose reveals a substantial fraction of double (nested) bars, probably in excess of 20–25%, and, in addition, that about 1/3 of barred galaxies host nested bars (Laine et al. 2001).

Probably the most intriguing property of nested bars is their theoretically anticipated stage of a dynamical decoupling, when each bar exhibits a different pattern speed (Shlosman, Frank, & Begelman 1989). Several aspects of this problem, which are closely related to the formation of double-bar systems and dynamical runaways there, are analyzed in the next section. Here we focus on the important characteristics of gas flow in double bars, presumed to tumble with pattern speeds $\Omega_s > \Omega_p$, where "p" stands for the primary (large-scale) bar and "s" for the secondary (sub-kpc) bar.

The gas response in nested bar systems has been never studied in detail. The first numerical simulations of double bars (Friedli & Martinet 1993; Heller & Shlosman 1994) were aimed at showing that bars can decouple. Elsewhere, in observational studies of nuclear bars, it was assumed that the properties of nuclear bars are identical to those of large-scale bars, in particular their gas dynamics and the appearance of characteristic offset dust lanes (e.g., Regan & Mulchaey 1999; Martini & Pogge 1999). But numerical simulations and general theoretical considerations support the view that nuclear bars are not scaled-down versions of large bars, and the gas response in nested bar systems differs profoundly from that in single bars (Shlosman & Heller 2001). This difference results from the underlying gravitational potential being time-dependent in all frames of reference, when bars tumble with different pattern speeds, and a number of other factors. In such cases the Jacobi energy (e.g., Binney & Tremaine 1987) is not an integral of motion even for a dissipationless "fluid", i.e., stars.

To understand the gas flow in time-dependent nested-bar potentials, one needs to study the dynamical constraints operating in these systems, such as conditions minimizing chaos. Pfenniger & Norman (1990) have pointed out that, in order to decrease the fraction of chaotic orbits in the system, corotation of the secondary bar must lie in the vicinity of the primary-bar ILR. This constrains Ω_s. Such a dynamical configuration, in principle, poses a problem for uninterrupted

gas inflow towards smaller radii. Namely, the gas flow is repelled at the bar corotation, inwards or outwards, because of the rim formed by the effective potential there, and hence may not cross the ILR/corotation radius (i.e., the bar–bar interface). Shlosman et al. (1989) have argued, in essence, that it is the gas self-gravity that overcomes such repulsion by modifying the underlying potential. In fact, even in the limit of neglibigle self-gravity in the gas, the flow is capable of crossing the bar–bar interface, but not in a steady manner and only for a restricted range of azimuthal angles (Shlosman & Heller 2001). Independently, one can analyze the conditions for shock and dust-lane formation in nuclear bars using a cloud–cloud collision model for the ISM and show that cloud properties and number densities should be extreme in order to maintain the cloud mean free path well below the nuclear bar width.

Modeling the Gas Response in Nested Bars Numerically, one can best study the gas response to the nested-bar potential by defining three regions in the disk: i) the primary-bar region (outside its ILR), ii) the bar–bar interface (hereafter the *interface*) encompassing the outer ILR of the large bar and the outer part of the secondary bar, and iii) the interior of the secondary bar. In the first region, the primary bar outside the interface, the gas responds by forming a pair of large-scale shocks, corresponding to the offset dust lanes, and flows inwards across the interface into the secondary bar. The flow in the primary bar, outside the interface, is steady and the shock strength and shape are nearly independent of time. Our analysis is limited to this time only and avoids transients.

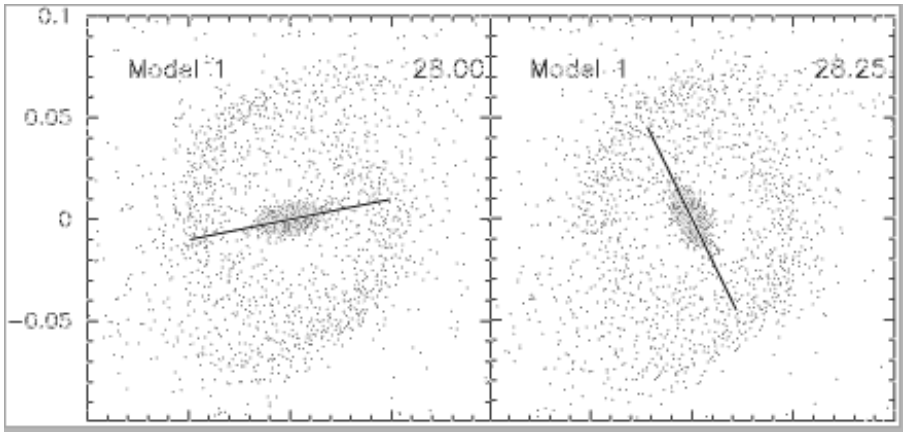

Figure 5. Snapshots of the gas density distribution in the central kpc (= 0.1): 2D SPH simulation in the background gravitational potential of a nested-bar disk galaxy (face on). The gas response to the bar torquing is shown in the primary bar (horizontal) frame of reference. Both bars and gas rotate counter-clockwise. The position angle of the secondary bar and its length are indicated by a *straight line*. Note that the nuclear bar lies within the nuclear ring. Time is given in units of dynamical time. (*From Shlosman & Heller 2001.*)

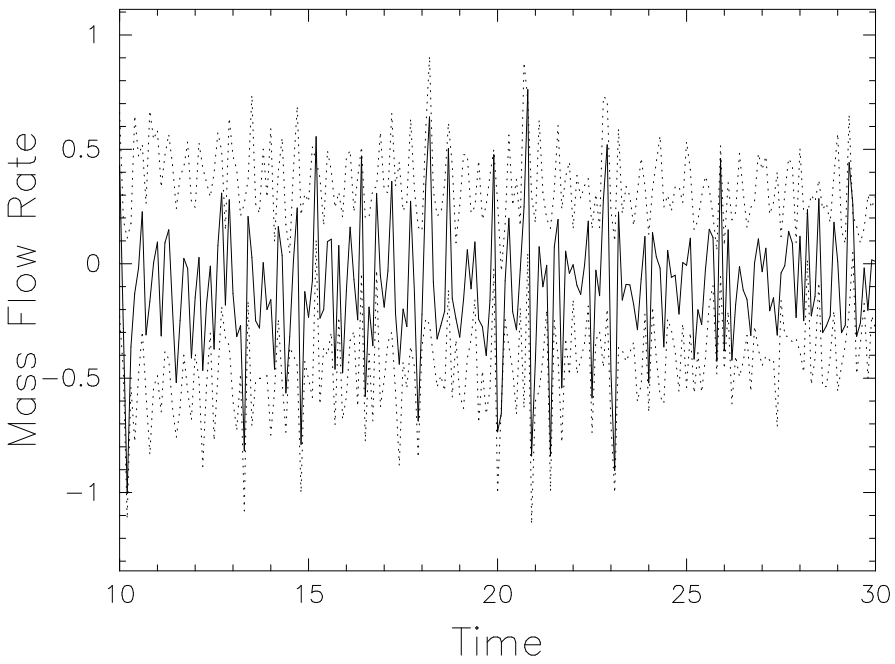

Figure 6. Time evolution of the gas inflow (negative) rate across the bar–bar interface of a double-bar system. *Upper dotted line:* Flow rate within ±45° of the major axis of the primary bar. *Lower dotted line:* Flow within ±45° of the minor axis of the primary bar. *Solid line:* Total flow across the bar–bar interface. Time is given in units of dynamical time.(*From Shlosman & Heller 2001.*)

In the second region, the bar–bar interface, the flow is time-dependent due to the perturbative effects of the secondary bar and changing background potential (Fig. 5). It correlates with the position angle of the secondary bar with respect to the primary bar or can be erratic. We have subdivided the azimuthal dependence of the gas flow into ±45° with the major axis of the primary bar and ±45° with its minor axis and Fourier-analyzed it. We found the beat frequency of the secondary bar for all models. But for smaller bars (i.e., short of their corotation) the amplitude of this Fourier component is lower and accompanied by other frequencies. For large nuclear bars (i.e., extending to their corotation), having a substantially stronger influence at the interface, the inflow shows the beat frequency clearly identified with the secondary bar tumbling (Fig. 6). *So the flow across the bar–bar interface depends upon the strength of the secondary bar*, ranging from chaotic, for a relatively weak perturbation of the secondary bar, to a more regular one. The corresponding mass influx rate is of the order of 0.3 $M_{\rm gas,9}\ M_\odot\ {\rm yr}^{-1}$, where $M_{\rm gas,9}$ is the total gas mass in the disk in units of $10^9\ M_\odot$ within the corotation of the large bar. On average, the inflow proceeds through the broad region along the primary-bar minor axis, while an outflow (albeit at a smaller rate) is directed along its major axis. The reason for this behavior is that the inflow is driven mainly along the large-scale shocks

penetrating the bar–bar interface from the primary bar. At the same time the outflow is detected at angles which do not encompass the large-scale shocks. The net effect is clearly an inflow across the corotation of the secondary bar.

The gas which is repelled by the secondary bar along the major axis of the primary bar is found to enter large-scale shocks while still moving out. This increases the mixing of material with different angular momentum increases inflow along the shocks. After crossing the bar interface the gas does not settle down but falls towards the third region, the inner 1/2–1/3 of the bar. Within this region the flow is very relaxed at all times, with uniform dissipation (well below the maximum dissipation in the large-scale shocks), and no evidence for grand-design shocks. In fact, we observe a kind of a "limb brightening" at the edge of this bar. This is seen in Fig. 7 as an enhanced density of above-average dissipating particles outside the oval-shaped central region and happens because the gas joins the bar from all azimuths.

The pattern of shock dissipation in nested bars can be inferred from Figure 7. It allows one to separate the incoming large-scale shocks from those driven by the secondary bar. Note that two systems of spiral shocks occur in Fig. 7, each associated with its corresponding bar. The large-scale (hereafter "primary") shocks extend to just pass off the minor axis of the primary bar, when the secondary bar is nearly orthogonal to the primary one. As it continues to tumble, the primary shocks extend deeper into the small bar. Sometime after both bars are aligned, the outer shocks detach themselves from the small bar, which is left with an additional pair of trailing shocks. This effect is especially pronounced between $t = 28.1$ and 28.2. To summarize, the interaction between these shock systems shows detachment when the bars are perpendicular and attachment when they are aligned with each other. The shapes of the shocks depend on the angle between the bars.

The Absence of Offset Shocks in Nuclear Bars A number of factors differentiate the gas dynamics in the decoupled secondary bars from that in the single bars. The first is the time-dependent nature of the gravitational potential in the nested-bar system during the dynamically decoupled phase. The second is the gas injection into the secondary bar which proceeds through the primary large-scale shocks penetrating the bar–bar interface. Such a phenomenon is absent at the corotation of the primary bars, which is depopulated of gas. A large amount of dissipation accompanying this process results in an inability of the gas to settle in the outer half of the secondary bar, which raises the question of whether the secondary bars can extend to their corotation.

The third factor is a fast secondary-bar pattern speed that does not permit secondary ILRs to form. If the decoupled phase of nested bars is short-lived, the quadrupole interaction between the bars will not be able to brake the small bar and form the ILRs. However, even in the case of a long-lived decoupled phase we do not expect nuclear bars to slow down, as the gas inflow across the interface and the resulting central concentration in fact speeds a bar up, as was found by Heller, Noguchi, & Shlosman (1993, unpublished). Because of the fast rotation, the x_1 orbits deep inside the secondary bars are round, with no loops or needle-shapes. The low-Mach-number gas flow is well organized here and capable of following these orbits with little dissipation, as shown in Figure 7. Non-linear orbit analysis reveals that the main orbits aligned with the secondary bar, x_1,

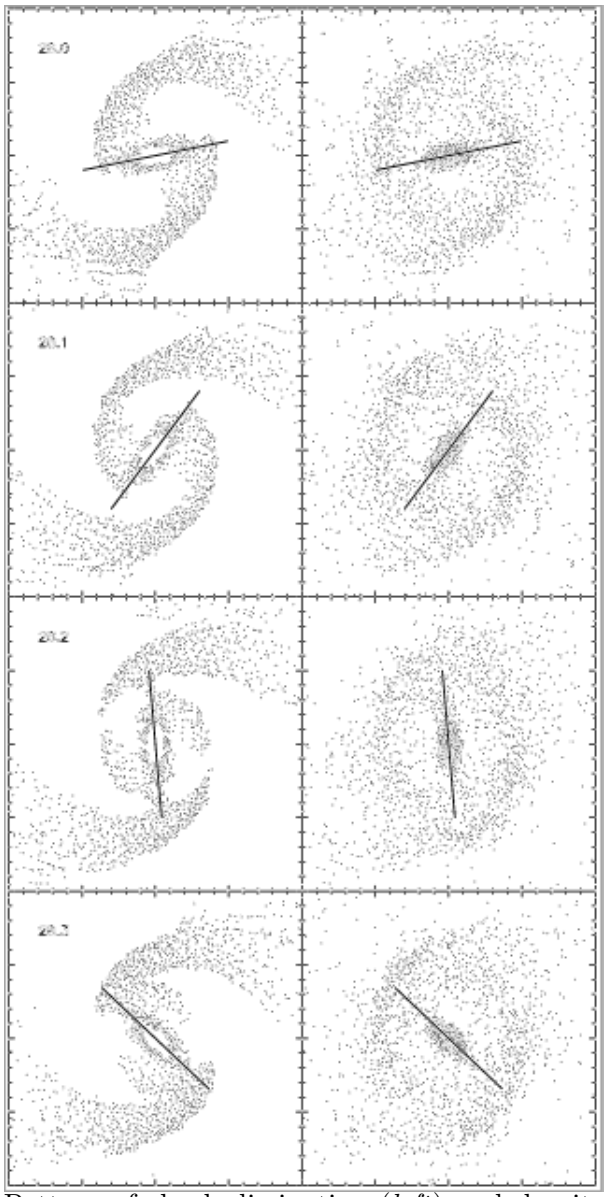

Figure 7. Pattern of shock dissipation (*left*) and density evolution (*right*) in the central kpc, shown in the frame of reference of the primary bar (horizontal). Positions of the secondary bar and its length are indicated by a *straight line*. All rotation is counter-clockwise. The particles on the *left* are those having a greater-than-average dissipation rate, which is given by the time derivative of the non-adiabatic component of internal energy. Note the sharply reduced dissipation in the innermost secondary bar and the "limb brightening" enveloping it. Also visible are two dissipative systems associated with the large-scale shocks in the primary bar and with the trailing shocks in the secondary bar. (*From Shlosman & Heller 2001.*)

have a mild ellipticity and no end-loops. This result is quite robust and holds despite the extreme axial ratio, 4 : 1, used here. No offset large-scale shocks form under these conditions.

Decoupled secondary bars avoid their ILRs because of their high pattern speeds. When ILRs are absent in a large-scale bar, the offset shocks weaken and recede to the major axis of the bar, becoming "centered" (e.g., Athanassoula 1992). They do not disappear completely because the underlying stellar periodic orbits have end-loops, are pointed, or have large curvature at the ends, forcing the gas to shock there. These orbital shapes result from the slower rotation of large, compared to nuclear, bars. Despite the fact that such weak centered shocks can exist theoretically, only two examples have been found from more than a hundred barred galaxies analyzed by Athanassoula (1992). During the last decade only one more potential example has been added to this list (Athanassoula, private communication). It seems plausible that centered shocks are very rarely observed because they are so weak.

Instead of "classical" centered shocks we find that the *inner* half of the secondary bars shows a rather uniform dissipation during the early stages of the gas inflow, which sharply decreases with time, or a "limb brightening" effect (Fig. 7). This dissipation is always small compared to dissipation in the primary large-scale shocks. Knapen et al. (1995) have analyzed the shock dissipation in a self-consistent gravitational potential of "live" stars and gas *before* the onset of decoupling, when both bars tumble with the same pattern speeds, and when the gas self-gravity is accounted for. No offset shocks have been found in this configuration either.

An important issue is the fate of the gas accumulating in the inner parts of the secondary bars. Under the observed conditions in numerical simulations (gas masses and surface densities) the gas self-gravity should exert a dominating effect on its evolution (see §4.2).

We conclude that no large-scale shocks and consequently no offset dust lanes will form inside secondary nuclear bars either when they are dynamically coupled and spin with the same pattern speeds as the primary bars, or when they are dynamically decoupled and spinning much faster. Two main factors, the time-dependent gravitational potential and the nature of the gas flow deep inside the bar, prevent the formation of these dust lanes. The time-dependent, "anisotropic" gas inflow across the ILR/corotation interface found here is a completely new phenomenon inherent to nested bars, because in single-barred systems no such inflow is possible at all *when the gas accumulation is small and its self-gravity is negligible*. The fate of the gas settling inside nuclear bars cannot be decided without invoking global self-gravitational effects in the gas that will completely change the nature of the flow there.

4. The Formation and Dynamical Decoupling of Nuclear Bars

Despite the obvious importance of the nested-bar configuration, our understanding of its formation, dynamics, and evolution is very limited. Even the sense of rotation of nuclear bars and their pattern speeds have never been detected directly from observations, although a number of projects are working on this.

Theoretically, three options exist. First, if the nuclear bar was formed via self-gravitational instability (in stellar or gaseous disks), it must spin in the direction given by the angular momentum in the disk, i.e., in the direction of the primary bar (Shlosman et al. 1989). In this case, the pattern speed of the nuclear bar, $\Omega_{\rm s}$, must be substantially *higher* than that of the primary bar, $\Omega_{\rm p}$, which has been confirmed in numerical simulations (Friedli & Martinet 1993; Combes 1994; Heller & Shlosman 1994). The presence of gas appears to be imperative for this to occur (e.g., Shlosman 1999). Both bars are dynamically *decoupled* and the angle between them in a face-on disk is arbitrary.

Second, two bars can corotate, being dynamically *coupled* and their rotation completely synchronized. Such a configuration can be a precursor to the future decoupled phase (discussed above), or continue indefinitely (e.g., the numerical simulations of Shaw et al. 1993; Knapen et al. 1995). The nuclear bar is expected to lead the primary bar in the first quadrant at a constant angle, close to 90°. An explanation for this phenomenon lies in the existence of two main families of periodic orbits, x_1 and x_2, in barred galaxies (see §2). The gas, losing angular support due to the gravitational torques from the primary bar, will flow towards the center and encounter the region with the x_2 orbits, which it will populate[1]. The extent of the x_2 family defines the inner resonance region in the disk, i.e., the position of the non-linear inner and outer ILRs. The nuclear bar may be further strengthened by the gas gravity, which drags stars into x_2 orbits. However, the amount of gas accumulating in the ILR resonance region may be insufficient to cause the dynamical runaway. In this latter case, it is thought that the synchronized system of two nearly perpendicular bars can be sustained indefinitely, until star formation or other processes act.

Third, the secondary bar can rotate in the opposite sense to the primary bar. This situation may arise from merging, when the outer galactic disk acquires opposite angular momentum to that of the inner disk. This was considered by Sellwood & Merritt (1994) and Davies & Hunter (1997) and appeared as a non-recurrent configuration. At least one of the bars should be purely stellar, because the gas cannot populate intersecting orbits.

Although all three options discussed above make specific predictions verifiable observationally, the triggering mechanism(s) for the formation of such systems require much better understanding. Much of the computational effort has so far gone into studying decoupling in self-gravitating (gas and stars) systems (e.g., Friedli 1999; Shlosman 1999). Unexpectedly, even non-self-gravitating gas can form a bar and decouple from the background potential (Heller et al. 2001). Following this work, we show that dynamical evolution does not stop with the formation of two coupled perpendicular bars, *even* when gas self-gravity is neglected. Instead, partial or complete decoupling of a nuclear gaseous bar, depending on the degree of viscosity in the gas, is triggered for a prolonged period of time. This bar either librates around the major axis of the primary bar, or acquires a different pattern speed, which is substantially *slower* than that of the primary bar. The role of gas self-gravity in the decoupling process is discussed

[1]Strictly speaking, the gas will not occupy perfectly periodic orbits because of dissipation, but will be found at nearby energies, which is sufficient for our discussion.

afterwards, and in this case $\Omega_s > \Omega_p$. Both regimes are likely to be encountered in nature and are therefore relevant to our understanding of galactic evolution.

4.1. Non-Self-Gravitating Nuclear Gaseous Bars

It is a common wisdom that a low-surface-density gas responds to single-bar torquing by forming a pair of offset shocks driving the gas towards the nuclear ring(s). Any further evolution stops here. Unexpectedly, we find that even non-self-gravitating gas can form a (gaseous) bar and decouple from the background potential, depending on the viscosity of the ISM (Heller et al. 2001).

The actual degree of viscosity in the ISM is difficult to estimate, partially due to its multiphase character. We have run three numerical models with identical initial conditions, with the sole difference that the value of the viscosity was changed by a factor of 2 above and below that of this standard model (hereafter "high" and "low" viscosity models). The gas was evolved using a 2D version of an SPH code (details in Heller & Shlosman 1994), neglecting the gas self-gravity and, alternatively, using the grid code ZEUS-2D (Stone & Norman 1992). Both numerical schemes gave similar results.

The most spectacular evolution occurred in the low-viscosity model, although all the models showed similar initial evolution during which, after forming a pair of large-scale shocks, the gas lost its angular momentum and accumulated in a double ring, corresponding roughly to the inner and outer ILRs. Furthermore, in all the models the rings interact hydrodynamically, destroying one of them. In the low viscosity model (Fig. 8), the inner ring is destroyed and its gas is mixed with the outer ring at intermediate radii. After merging, a single oval-shaped ring corotates with the primary bar, leading it by $\phi_{\rm dec} \sim 50^\circ$ (the so-called decoupling angle, whose value depends on the gas viscosity).

Subsequently, the remaining ring (in all the models) becomes increasingly oval and barlike (see eccentricity evolution for low viscosity model in Fig. 9), its pattern speed changes abruptly, and it swings towards the primary bar, *against* the direction of rotation of this bar. We describe the evolution of this gas flow in terms of the bar dynamics and call it a *nuclear gaseous bar*. (In the inertial frame, the nuclear bar still spins in the same direction as the main bar, albeit with a smaller pattern speed than Ω_p.) The shape of this bar can be described by its axial (minor-to-major) ratio, which reaches a minimum when both bars are aligned. After crossing the primary-bar axis into the fourth quadrant, the nuclear bar initially decreases its axial ratio, i.e., it becomes less oval. Thereafter it stops, becomes more oval, and speeds up in the prograde direction. The bar axial ratio reaches its minimum when both bars are aligned and the gaseous bar rotates in the retrograde direction (in the primary-bar frame!).

In standard and high-viscosity models, the nuclear bar librates about the primary bar with a decreasing amplitude, being damped more strongly in the latter model. The low-viscosity model, however, behaves in a qualitatively different way. Instead of librating about the primary bar, the nuclear bar continues to swing in the same direction maintaining a pattern speed $\Omega_s < \Omega_p$ for about 60 dynamical times, corresponding in our units to about 2–3 $\times 10^9$ yr. On average, its pattern speed is about half of Ω_p, oscillating around this value with a substantial amplitude. At times, Ω_s is very small, giving the impression that the nuclear bar stagnates in the inertial frame of reference. With time, the ec-

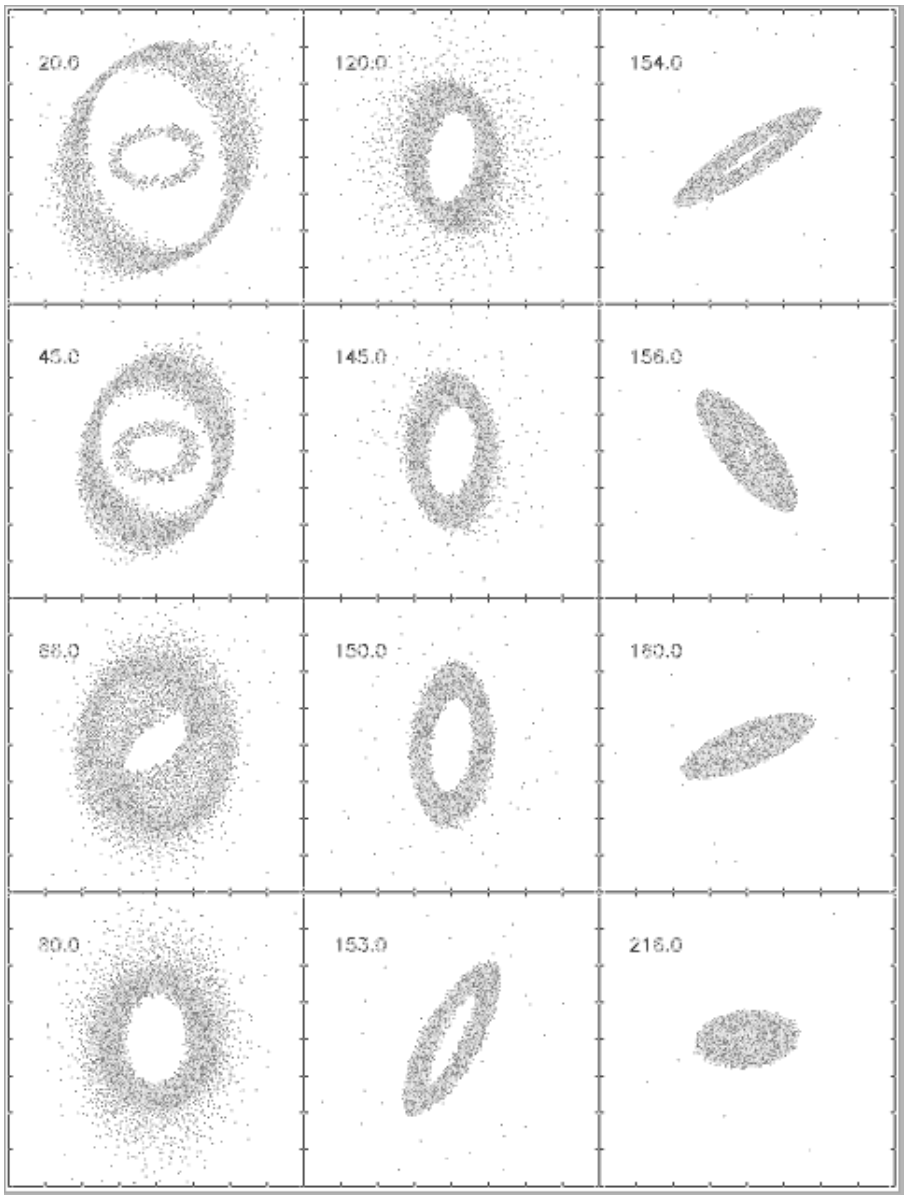

Figure 8. Time evolution of the low-viscosity model: 2D SPH simulation in the background gravitational potential of a barred disk galaxy (shown face on). The gas response to the bar torquing is displayed in the primary-bar frame. The primary bar is horizontal and the gas rotation is counter-clockwise. Note a fast evolution after $t \sim 150$, when the nuclear bar decouples and swings clockwise (!). The bar is "captured" again at $t \sim 211$. Time is given in units of dynamical time, $\tau_{\rm dyn}$. The animation sequence discussed here and others are available in the online edition of Heller et al. (2001).

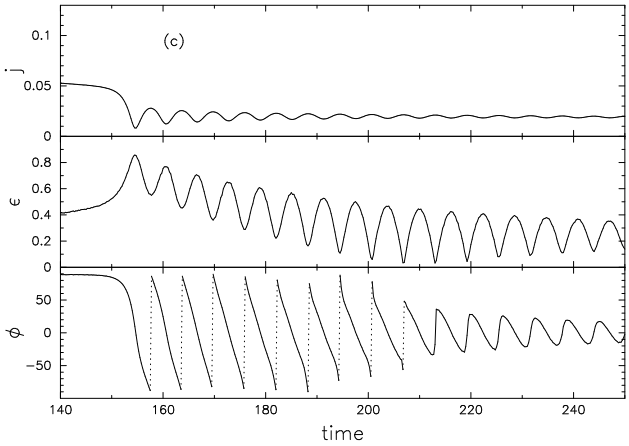

Figure 9. Low-viscosity model (see also Fig. 8): evolution of total specific angular momentum j in the primary-bar frame of reference (*upper*), eccentricity $\epsilon = 1 - b/a$ (*middle*), and position angle, ϕ, of the line of apsides (*lower*) of the gaseous nuclear bar. Both ϕ and ϵ were computed from the tensor of inertia of the gas within the small bar. The time is given in units of dynamical time. The angle ϕ is shown between $\pm\pi/2$ for presentation only and discontinuities are marked by *vertical dotted lines*. Full decoupling of the nuclear bar exists at $\tau \approx$ 150–211.

centricity of the nuclear bar gradually decreases and the bar is trapped again by the valley of the potential of the main bar, thus entering the libration phase, similar to other models.

What are the physical reasons for the partial or complete runaways shown in each model? Looking at the distribution of gas particles in the rings with Jacobi energy, $E_{\rm J}$, one finds that after merging the ring is positioned close to the energy where the transition from x_2 to x_1 (at the inner ILR) occurs. The exact value of this transition energy is model-dependent of course, but this is of no importance to the essence of the decoupling.

Viscosity is most important during the phase when both rings interact hydrodynamically and merge, which understandably starts earlier and proceeds faster for higher-viscosity models. This pre-decoupling evolution is similar in all models, apart from the timescale. The crucial difference between the models comes from 1) the position of the nuclear bar on the $E_{\rm J}$ axis after merging and 2) the value of the $\phi_{\rm dec}$ angle, i.e., the orientation of the nuclear bar at the time of decoupling. We note that the role of viscosity here is fundamentally different from that in nearly axisymmetric potentials (planetary rings, galactic warps, etc.), where it acts to circularize the orbits. In barred potentials, circular orbits do not exist and the gas merely moves from one elongated orbit to another.

The single remaining ring is subject to a gravitational torque from the primary bar, which acts to align the ring with the bar. In the pre-decoupling stage, the ring becomes progressively barlike, decreasing its axial ratio. In the low-viscosity model, this gaseous bar resides in purely x_2 orbits and, therefore,

responds to the primary-bar torque by speeding up its precession while being pulled backwards until it is almost at right angles to the bar potential valley. The decoupling happens abruptly when a substantial fraction, $\sim 1/2$, of the gas in the bar finds itself at $E_{\rm J}$ energies below the inner ILR. The absence of x_2 orbits at these $E_{\rm J}$ means that the bars either are unable to settle on these orbits or lose their stable orientation along the primary-bar minor axis. As a result, the nuclear bars enter into libration about the main bar with smaller or larger initial departures from the stable orientation along the main bar, *which is a single decisive factor separating the partial and full decouplings*.

The angle $\phi_{\rm dec}$ is largest for the low-viscosity model—the reason for the qualitatively different behavior. All three models show that gaseous bars in the partial or full decoupling phase experience shape changes depending on their orientation. The bar has a much smaller eccentricity in the fourth quadrant than in the first (Fig. 9). Such an asymmetry with respect to the primary-bar axis ensures that the resulting gravitational torques from the primary bar are smaller in the fourth quadrant. But only for the least viscous model, which has the maximal $\phi_{\rm dec}$, does this make the ultimate difference. In this case the torques are unable to confine the bar oscillation, which continues for a full swing of 2π. The nuclear bar is trapped again at $\tau \sim 211$, after many rotations with respect to the large-scale bar.

The clear correlation between the eccentricity of the nuclear bar and its angle with the primary bar in the decoupled phase shown by *all* the models can be tested observationally, e.g., by looking at the molecular rings in CO. The maximum in the gaseous bar eccentricity, ϵ, is achieved each time both bars are aligned and the minimum occurs when the bars are at right angles.

Two additional effects should have observational consequences as a corollary to decoupling and the periodic increase in ϵ. First, the gas will move inwards across the inner ILR on a dynamical timescale. Shlosman et al. (1989) pointed out that ILR(s) present a problem for radial gas inflow because the gas can stagnate there. A solution was suggested in the form of a global self-gravitational instability in the nuclear ring or disk, which will generate gravitational torques in the gas, driving it towards the nuclear region.

Recently Sellwood & Moore (1999) resurrected the idea that ILRs would "choke" the gas inflow. However, as we see here, even non-self-gravitating nuclear rings are prone to dynamical instability which drives the gas inwards, whether in a full or partial decoupling. Second, this instability can be accompanied by star formation along the molecular bar due to increased dissipation in the gas, and this star formation will have a quasi-periodic bursting character.

4.2. Self-Gravitating Nuclear Gaseous Bars

Gas self-gravity plays a crucial role in the formation and dynamical decoupling of secondary, nuclear, bars. In this case $\Omega_{\rm s} > \Omega_{\rm p}$ (Shlosman et al. 1989). Numerical simulations which directly tackle the decoupling issue in this regime have been very limited so far. Friedli & Martinet (1993, and priv. communication) also experienced difficulties in decoupling pure stellar disks. As mentioned above, the inner stellar bar in this case is very transient and quickly dissappears, although this may be a result of an insuffient number of particles. Combes (1994) was unable to obtain decoupling in the purely stellar *and* gaseous cases. For a

mixed system of gas and stars, the decoupled stage is more prolonged. Hence, numerical simulations clearly favor decoupling in the non-linear stage and explicitly demonstrate the necessity for gas to be present, in addition to the stellar component.

Numerical simulations also confirm that an increased central-mass concentration is important for the dynamical separation of the outer and inner parts. This can be only achieved by moving the gas by means of a large-scale stellar bar. The gas accumulates inside the ILR in the x_2 orbits, modifying the local potential and ultimately forming a double ILR. The gravity of the gas settling into these orbits is sufficient to "drag" the stars along and twist the NIR isophotes (e.g., Shaw et al. 1993), but such a configuration still corotates with the stellar bar. The ability of the gas to settle into the x_2 orbits depends upon its sound speed and viscosity. When the gas is too viscous or too hot, it will avoid the ILRs completely and remain in the x_1 orbits aligned with the bar (Englmaier & Gerhard 1997; Englmaier & Shlosman 2000; Patsis & Athanassoula 2000). Moderately viscous gas will settle into the innermost x_2 orbits, losing angular momentum due to viscous torques in addition to the gravitational torques from the bar. The evolution of nuclear regions in disks, therefore, depends on the (unknown) equation of state of the ISM. The inclusion of star formation in nuclear rings has already demonstrated how the resulting increase in viscosity leads to the mass transfer across the ILRs, as evident from Figure 2.

Alternatively, Englmaier & Shlosman (1999, unpublished) have modified the ZEUS-2D hydrocode (Stone & Norman 1992) to study the stability and evolution of nuclear rings discussed in §4.1, in the presence of gravitational effects in the gas. In the first stage, the nuclear rings started to librate around the potential valley of the stellar bar. However, almost immediately the rapid growth of self-gravitating modes with $m = 2$ and 4 has led to the appearance of a prograde mode (i.e., in the direction of gas rotation) with pattern speed much larger than $\Omega_{\rm p}$. This has resulted in an avalanche-type flow towards smaller radii. A model with the central SBH revealed that inflowing gas feeds the SBH at peak rates, increasing its mass tenfold. The exact analysis of unstable global modes in these configurations is under way, in particular their relationship to I and J modes found in Christodoulou & Narayan (1992) and Christodoulou (1993), and to stability of the Maclaurin sequence of self-gravitating rotating fluids (Christodoulou et al. 1995).

A big unknown is the concurrent star formation, which was neglected in these simulations. Note, however, that the star formation has low efficiency and can hardly halt this runaway collapse toward the center.

5. Final Remarks

The central kpc of disk galaxies can host a number of non-axisymmetric morphological features, from mild perturbations, such as nuclear spirals driven by large-scale bars, to triaxial bulges, to strong secondary bars, gaseous or stellar. Their effects on the dynamics of the ISM and its state are complex and require a long-range effort in order to understand the central activity, which includes massive star formation and fueling of the central SBHs. New observations indicate that the state of the cold-phase ISM within the central kpc may differ from

that in the surrounding disk (e.g., Hüttemeister & Aalto, this volume, p. 617) and numerical simulations reveal little analogy between the gas dynamics in the central regions and in the outer disks.

New higher-resolution numerical simulations involving much larger amounts of particles will clarify the issues related to nested bar formation and self-gravitating gas dynamics in these systems. Coupled with new observational techniques and instruments at longer wavelengths, they will shed light on the intricate evolution of central regions within the general context of cosmological evolution.

Acknowledgments. I am grateful to my collaborators Peter Englmaier, Clayton Heller, Johan Knapen, Seppo Laine, and Reynier Peletier. I thank the organizers of this conference for financial assistance. This work is supported in part by NASA grants NAG 5-10823, HST GO-08123.01-97A, and WKU-522762-98-6.

References

Athanassoula, E. 1992, MNRAS, 259, 345

Binney, J., & Tremaine, S. 1987, Galactic Dynamics (Princeton: Princeton University Press)

Buta, R., & Crocker, D. A. 1993, AJ, 105, 1344

Christodoulou, D. M. 1993, ApJ, 412, 696

Christodoulou, D. M., Kazanas, D., Shlosman, I., & Tohline, J. E. 1995, ApJ, 446, 510

Christodoulou, D. M., & Narayan, R. 1992, ApJ, 388, 451

Combes, F. 1994, Mass-Transfer Induced Activity in Galaxies, ed. I. Shlosman (Cambridge: Cambridge University Press), p. 170

Contopoulos, G., & Papayannopoulos, T. 1980, A&A, 92, 33

Davies, C. L., & Hunter J. H., Jr. 1997, ApJ, 484, 79

de Vaucouleurs, G. 1974, in IAU Symp. 58, The Formation and Dynamics of Galaxies, ed. J.R. Shakeshaft (Dordrecht: Reidel), p. 335

de Vaucouleurs, G., de Vaucouleurs, A., Corwin H. G., Jr., Buta, R., J., Paturel, G., & Fouque, P. 1991, 3rd Reference Catalogue of Bright Galaxies (New York: Springer)

Devereux, N. A., Kenney, J. D. P., & Young, J. S. 1992, AJ, 103, 784

Elmegreen, B. G. 1994, ApJ, 425, L73

Elmegreen, B. G., & Elmegreen, D. M. 1985, ApJ, 288, 438

Elmegreen, D. M., Chromey, F. R., & Santos, M. 1998, AJ, 116, 1221

Emsellem, E., Greusard, D., Combes, F., Friedli, D., Leon, S., Pécontal, E., & Wozniak, H. 2001, A&A, 368, 52

Englmaier, P., & Gerhard, O. 1997, MNRAS, 287, 57

Englmaier, P., & Shlosman, I. 2000, ApJ, 528, 677

Erwin, P., & Sparke, L. S. 1999, ApJ, 521, L37

Friedli, D. 1999, ASP Conf. Ser., vol. 187, Evolution of Galaxies on Cosmological Timescales, ed. J. E. Beckman & T. J. Mahoney, eds. (San Francisco: ASP). p. 88

Friedli, D., & Martinet, L. 1993, A&A, 277, 2

Friedli, D., Wozniak, H., Rieke, M., Martinet, L., & Bratschi, P. 1996, A&AS, 118, 461

Heller, C. H., & Shlosman, I. 1994, ApJ, 424, 84

Heller, C. H., & Shlosman, I. 1996, ApJ, 471, 143

Heller, C. H., Shlosman, I., & Englmaier, P. 2001, ApJ, 553, 661

Ishizuki, S., Kawabe, R., Ishiguro, M., Okumura, S. K., & Morita, K.-I. 1990, Nat, 344, 224

Jogee, S., Kenney, J. D. P., & Smith, B. J. 1998, ApJ, 494, L185

Jungwiert, B., Combes, F., & Axon, D. J. 1997, A&AS, 125, 479

Knapen, J. H., Beckman, J. E., Heller, C. H., Shlosman, I., & de Jong, R. S. 1995, ApJ, 4, 623

Knapen, J. H., Shlosman, I., & Peletier, R. F. 2000, ApJ, 529, 93

Kormendy, J. 1982, ApJ, 257, 75

Kotilainen, J. K., Reunanen, J., Laine, S., & Ryder, S. D. 2000, A&A, 353, 834

Laine, S., Knapen, J. H., Perez-Ramirez, D., Doyon, R., & Nadeau, D. 1998, MNRAS, 302, 33L

Laine, S., Shlosman, I., Knapen, J. H., & Peletier, R. F. 2001, ApJ, in press (astro-ph/0108029)

Maiolino, R., Alonso-Herrero, A., Anders, S., Quillen, A., Rieke, M. J., Rieke, G. H., & Tacconi-Garman, L. E. 2000, ApJ, 531, 219

Martini, P., & Pogge, R. W. 1999, AJ, 118, 2646

Mulchaey, J. S., & Regan, M. W. 1997, ApJ, 482, L135

Patsis, P. A., & Athanassoula, E. 2000, MNRAS, 358, 45

Pfenniger, D., & Norman, C. A. 1990, ApJ, 363, 391

Prendergast, K. H. 1962, Distribution and Motion of ISM in Galaxies, ed. L. Woltjer (New York: Benjamin), p. 217

Regan, M. W., & Mulchaey, J. S. 1999, AJ, 117, 2676

Sandage, A., & Brucato, R. 1979, AJ, 84, 472

Sellwood, J. A., & Merritt, D. 1994, ApJ, 425, 530

Sellwood, J. A., & Moore, E. M. 1999, ApJ, 510, 125

Shaw, M. A., Axon, D. J., Probst, R., & Gatley, I. 1995, MNRAS, 274, 369

Shaw, M. A., Combes, F., Axon, D. J., & Wright, G. S. 1993, A&A, 273, 31

Shlosman, I. 1999, ASP Conf. Ser., vol. 187, Evolution of Galaxies on Cosmological Timescales, ed. J. E. Beckman & T. J. Mahoney, (San Francisco: ASP), p. 100

Shlosman, I., Frank, J., & Begelman, M. C. 1989, Nat, 338, 45

Shlosman, I., & Heller, C. H. 2001, ApJ, submitted

Stone, J. M., & Norman, M. L. 1992, ApJS, 80, 753

Discussion

Beckman: So is the object we have just seen a bar or a ring?

Shlosman: Gaseous bars are basically very elongated rings. This is the only way to avoid the intersecting orbits which gas can*not* populate. In the case of intersecting orbits, this would limit the bar lifetime to a fraction of a rotation period.

Beckman: Your movie showed the inner bar with a *slower* pattern speed than the main bar, but are the observations not showing that the nuclear bars have higher pattern speeds?

Shlosman: Pattern speeds of nuclear bars, either stellar or gaseous, have not yet been determined. We have presented for the first time an instability in a gaseous ring which leads to a pattern speed slower than that of the primary stellar bar.

Elmegreen: Why do the stars that are born in a gaseous inner ring stay in the ring long after star formation is over and the gas is dispersed (as we heard from Peter Erwin this morning)? This implies that gas dynamical processes do not define the equilibrium gaseous ring position, but only gravity does.

Shlosman: This is hardly surprising. There are a number of possibilities for removing the gas from the original position of the nuclear ring. First, the bar instability in a weakly self-gravitating gas shown in our work removes a sufficient amount of angular momentum and energy (i.e., Jacobi energy) from the gas transferring it deeper into the potential well. If stars coexisted initially with the gas, they would go through the same process. In other words, stars stay where they form at their original (Jacobi) energies. We have checked the dynamical evolution of such a stellar ring and found that it thickens initially due to the differential precession of individual stellar orbits, and then any dynamical evolution slows down dramatically. So the red nuclear stellar rings mentioned before (Shlosman 1999) are a normal product of the cut-off of the gas supply to the ring (e.g., due to bar weakening or the absence of available gas).

Norman: Does the final state of the inner bar have the same pattern speed as the outer primary bar?

Shlosman: The dynamical decoupling is always limited in time and to particular cases (stellar, gaseous, or mixed decouplings). The instability discussed here, leading to the decoupling of a low-surface-density (weakly self-gravitating) gas results in pattern speeds that are *lower* by a factor of 2–3 than the pattern speed of the primary stellar bar.